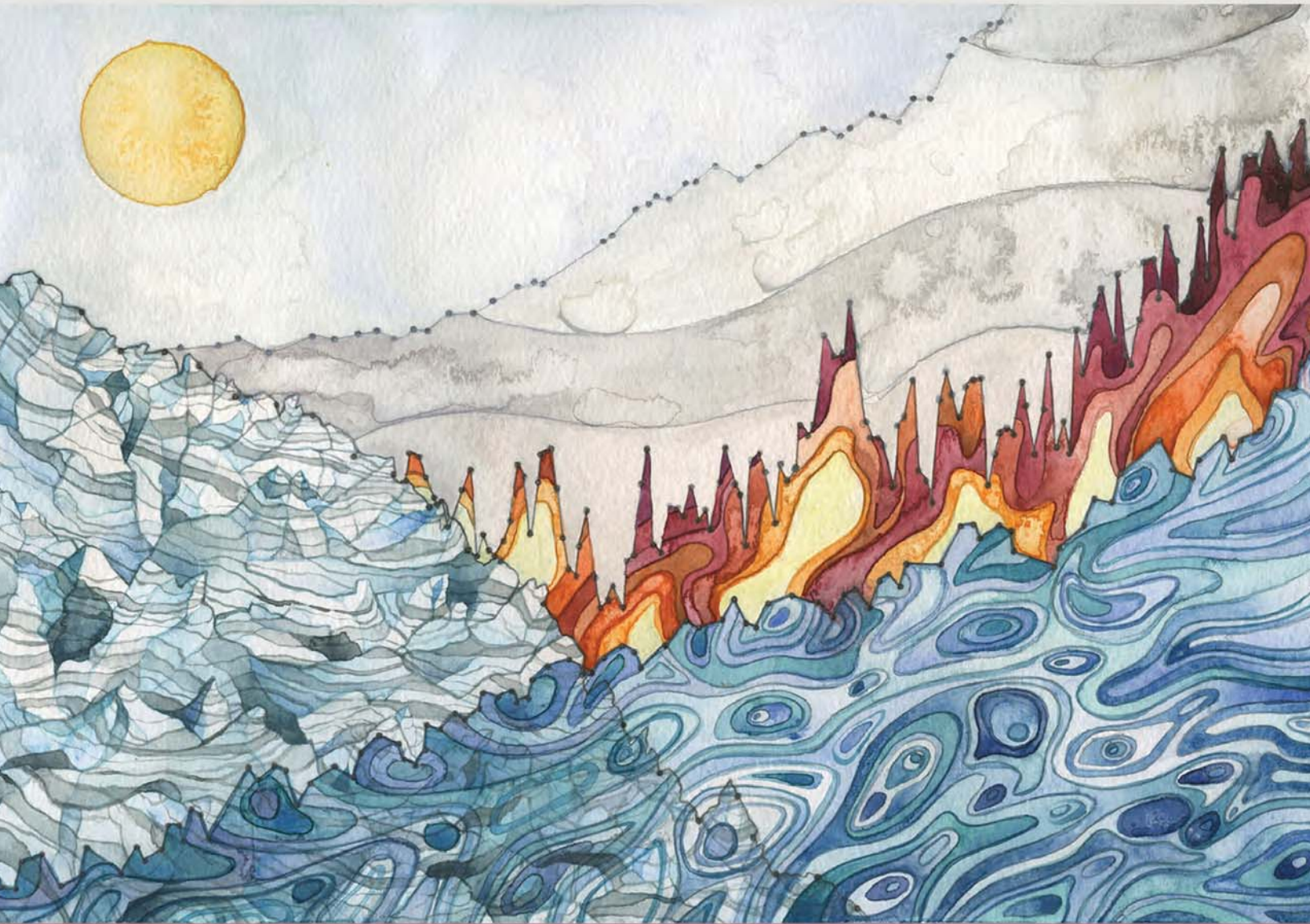
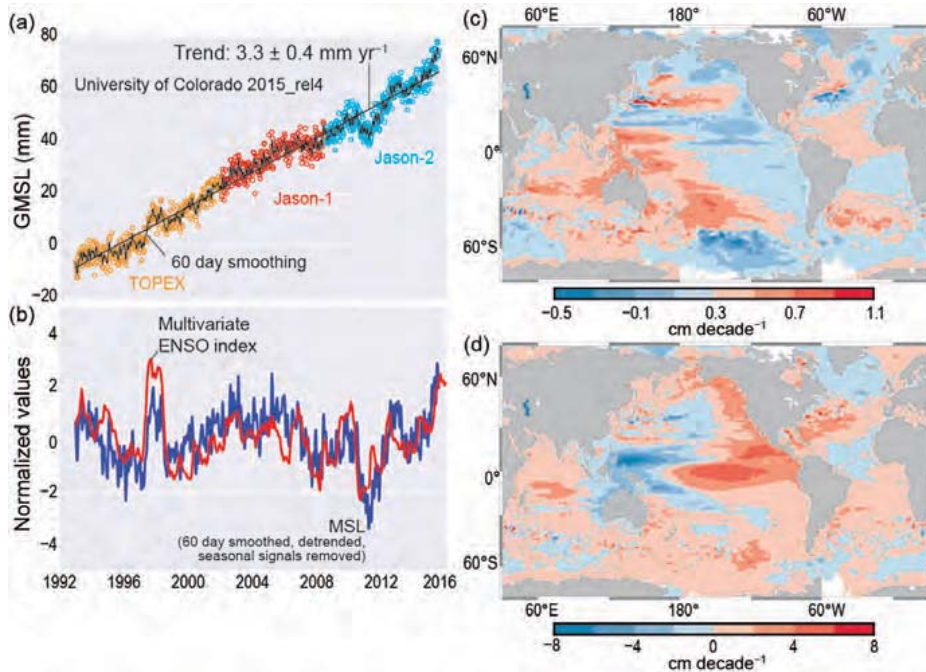


# STATE OF THE CLIMATE IN 2015



Special Supplement to the  
*Bulletin of the American Meteorological Society*  
Vol. 97, No. 8, August 2016



**FIG. 3.17.** (a) Global mean sea level (mm) obtained from consecutive satellite altimeter missions, with 60-day smoothing and seasonal signals removed (black line indicates a rise rate of  $3.3 \text{ mm yr}^{-1}$ ); (b) Detrended GMSL compared with the multivariate ENSO index (MEI; obtained from <http://sealevel.colorado.edu>); (c) Sea level trends ( $\text{cm decade}^{-1}$ ) 1993–2015; and (d) Sea level trends ( $\text{cm decade}^{-1}$ ) 2011–15. Scales differ in (c) and (d).

*g. Surface currents*—R. Lumpkin, G. Goni, and K. Dohan

Ocean surface current changes, transports derived from ocean surface currents, and features such as rings inferred from surface currents, all play a role in ocean climate variations. Surface currents described here are obtained from in situ (global array of drogued drifters and moorings) and satellite (altimetry, wind stress, and SST) observations. Transports are derived from a combination of sea level anomalies (from altimetry) and climatological hydrography. For details of these calculations, see Lumpkin et al. (2011). Anomalies are calculated with respect to 1992–2007. Annually averaged zonal current anomalies for 2015, changes in anomalies from 2014 to 2015 (Fig. 3.19), and seasonal average 2015 anomalies (Fig. 3.20) are discussed below by individual ocean basin.

The dramatic El Niño of 2015/16 dominated annual mean current anomalies in the Pacific basin (Fig. 3.19a), with annually averaged eastward anomalies  $>20 \text{ cm s}^{-1}$  between  $1.5^\circ$  and  $6^\circ\text{N}$  and weaker eastward anomalies in the rest of the latitude band between  $10^\circ\text{S}$  and  $10^\circ\text{N}$ . Because 2014 was characterized by westward anomalies on the equator and eastward anomalies in a strengthened North Equatorial Countercurrent (NECC) at  $5^\circ$ – $6^\circ\text{N}$ , the 2015 minus 2014 map (Fig. 3.19b) has larger eastward anomaly tendencies on the equator and weaker

tendencies along the NECC than the 2015 anomaly map (Fig. 3.20).

In contrast to the annual mean picture, 2015 began with westward anomalies between  $5^\circ\text{S}$  and  $5^\circ\text{N}$  across the eastern half of the basin (Fig. 3.20a), with peak westward anomalies of  $\sim 25 \text{ cm s}^{-1}$  at  $1^\circ\text{N}$ . These anomalies were an enhancement of the northern branch of the westward South Equatorial Current (SEC) as seen in December 2014 (Dohan et al. 2015). Immediately north of  $5^\circ\text{N}$ , the eastward NECC was only marginally faster than its climatological January strength. In February, intense El Niño-related eastward anomalies first appeared in the western tropical Pacific as anomalies of  $20$ – $40 \text{ cm s}^{-1}$  at  $145^\circ$ – $175^\circ\text{E}$ ,  $2.5^\circ\text{S}$ – $4^\circ\text{N}$ .

Throughout boreal spring, the El Niño-related anomaly pattern propagated eastward (Fig. 3.20b), reaching  $160^\circ\text{W}$  by March and  $90^\circ\text{W}$  by April. During these months, warm water advected by these current anomalies caused the NINO3 and NINO3.4 SST indices to increase rapidly (see section 4b). In April, eastward anomalies of  $40$ – $50 \text{ cm s}^{-1}$  were present at  $95^\circ$ – $130^\circ\text{W}$ ,  $2.5^\circ\text{S}$ – $2.5^\circ\text{N}$ . Throughout March and April, equatorial zonal currents in the band  $120^\circ\text{W}$ – $180^\circ$  were close to their climatological average, straddled by the eastward anomalies centered at  $5^\circ$ – $6^\circ\text{N}$  (the latitude of the NECC) and  $1^\circ$ – $2^\circ\text{S}$  (Fig. 3.20b). In May, the anomalies south of the equator diminished to  $<20 \text{ cm s}^{-1}$ , while anomalies of  $35$ – $40 \text{ cm s}^{-1}$  persisted in the NECC band. The eastward advection of relatively fresh water, combined with an El Niño-driven shift in the ITCZ (section 3e), likely accounts for the development of fresh SSS anomalies (section 3d).

Throughout boreal summer (June–August; Fig. 3.20c), eastward anomalies persisted across the basin, with equatorial eastward anomalies returning across the western half of the basin in July and across the entire basin in August. Averaged over these three months (Fig. 3.20c), eastward anomalies exceeded  $5 \text{ cm s}^{-1}$  from  $6^\circ\text{S}$  to  $9^\circ\text{N}$ , with peak anomalies of  $30$ – $35 \text{ cm s}^{-1}$  at  $4^\circ$ – $6^\circ\text{N}$ . This pattern persisted in boreal

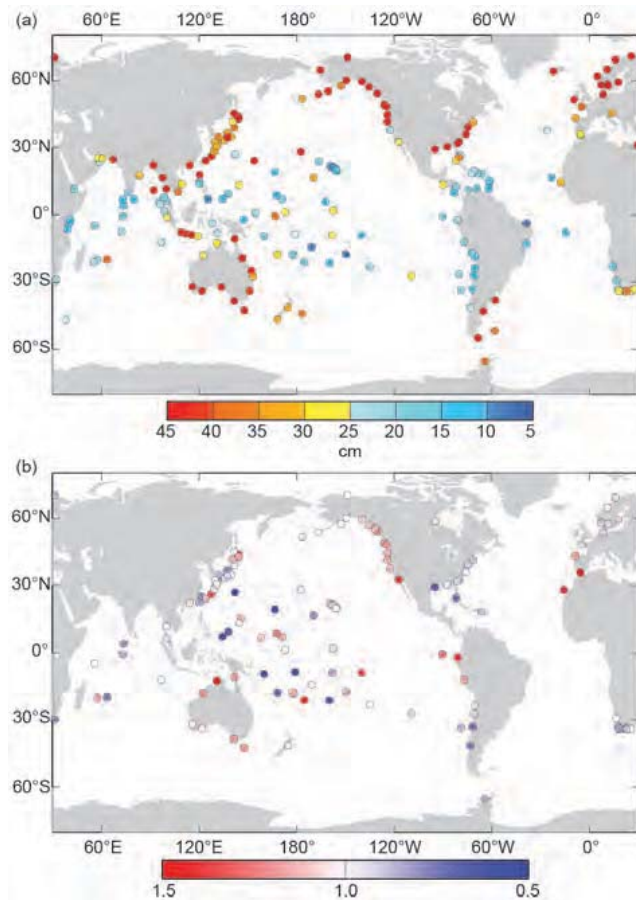


**FIG. 3.18. (a) Annual maximum sea level (cm) during 2015 computed from the mean of the 2% highest daily values relative to the 2015 annual mean, measured at tide gauges (<http://uhslc.soest.hawaii.edu>); (b) The 2015 annual maximum from (a) divided by the time-averaged annual maximum measured at each station with at least 20 years of data.**

autumn (Fig. 3.20d), with another pulse of extremely strong ( $>50 \text{ cm s}^{-1}$ ) eastward anomalies appearing at  $170^{\circ}\text{E}$ – $150^{\circ}\text{W}$ ,  $3^{\circ}$ – $5^{\circ}\text{N}$  in August and peaking at  $>60 \text{ cm s}^{-1}$  in October; these were the strongest monthly averaged broad-scale current anomalies seen in 2015. This pattern propagated eastward in November and weakened significantly through December. The year concluded with eastward anomalies of  $\sim 20 \text{ cm s}^{-1}$  across the basin from  $3^{\circ}\text{N}$  to  $6^{\circ}\text{N}$ , consistent with a stronger and wider NECC than in the December climatology. The northern edge of this NECC was close to its climatological northern extent but extended south to  $2^{\circ}\text{N}$ , compared to  $3.5^{\circ}\text{N}$  in climatology.

The Kuroshio was shifted anomalously northward in 2010–14, although this shift diminished during 2014 (Dohan et al. 2015). During 2015, the Kuroshio was close to its climatological latitude, with a maximum annually averaged speed of  $35 \text{ cm s}^{-1}$  at  $35^{\circ}\text{N}$  between  $140^{\circ}$  and  $170^{\circ}\text{E}$  (Fig. 3.19).

Surface current anomalies in the equatorial Pacific typically lead SST anomalies by several months, with a magnitude that scales with the SST anomaly magnitude. A return to normal current conditions is also typically seen before SST returns to normal. Thus, current anomalies in this region are a valuable predictor of the evolution of SST anomalies and their related climate impacts. This leading nature can be seen in the first principal empirical orthogonal function (EOF) of surface current (SC) anomaly and separately of SST anomaly in the tropical Pacific basin (Fig. 3.21). For 1993–2015, the maximum correlation between SC and SST is 0.70 with SC leading SST by 71 days. Both SC and SST EOF amplitudes were positive throughout 2015, with the cumulative effect of positive SC EOF amplitude resulting in a steadily increasing SST EOF amplitude to almost 3 standard deviations in November 2015, nearing the November 1997 value of 3.2.

Throughout most of 2015, Indian Ocean monsoon-driven currents were much closer to climatology than the dramatic anomalies seen in the Pacific (Fig. 3.19a). This normality is in contrast to the strong eastward anomalies seen across the basin in 2013–14 (Lumpkin et al. 2014; Dohan et al. 2015). Those eastward anomalies dominate the 2015 minus 2014

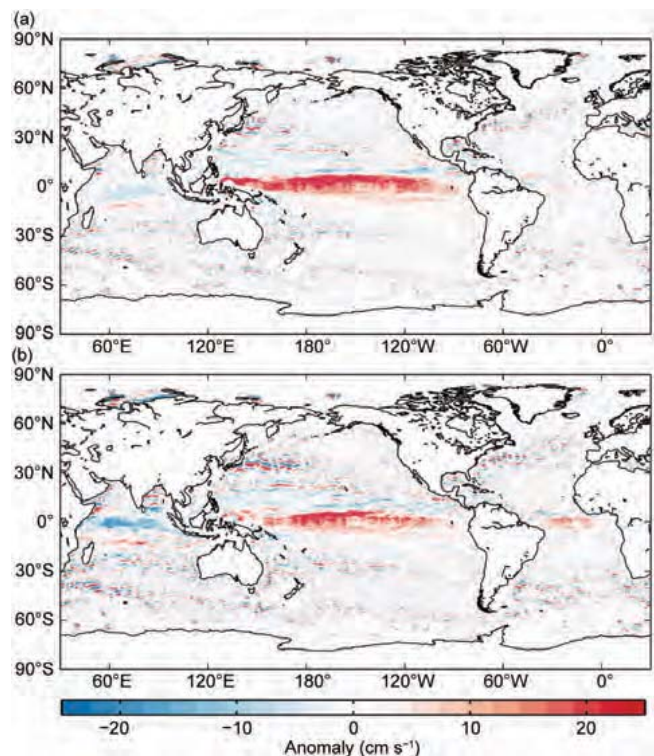


**FIG. 3.19. Annually averaged geostrophic zonal current anomalies ( $\text{cm s}^{-1}$ ) for (a) 2015 and (b) 2015 minus 2014 derived from a synthesis of drifters, altimetry, and winds. Positive (red) values denote anomalously eastward velocity.**

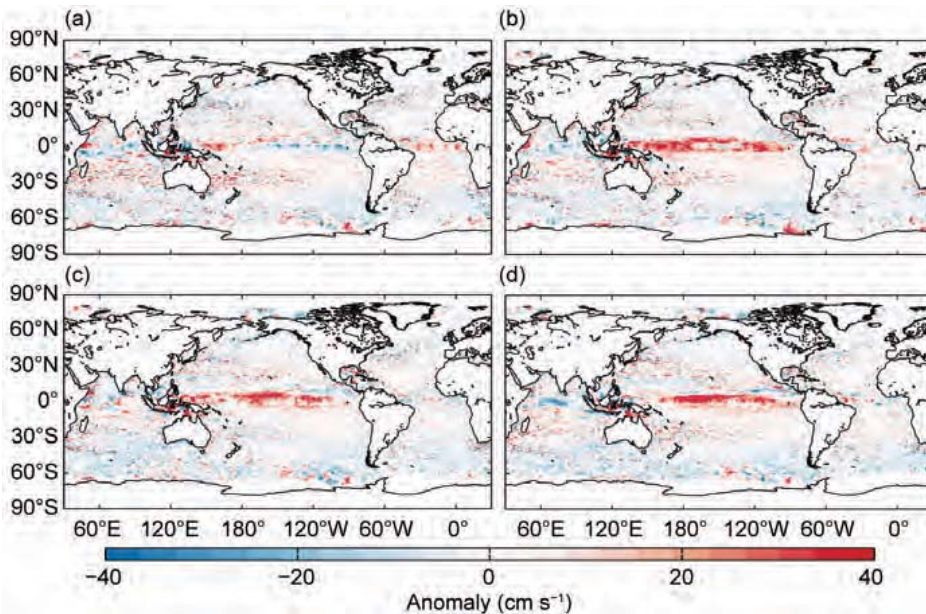


**FIG. 3.20. Seasonally averaged zonal geostrophic anomalies ( $\text{cm s}^{-1}$ ) with respect to seasonal climatology, for (a) Dec 2014–Feb 2015, (b) Mar–May 2015, (c) Jun–Aug 2015, and (d) Sep–Nov 2015.**

zonal current tendencies in the Indian Ocean basin (Fig. 3.19b). In 2015, the strongest anomalies with respect to monthly climatology were seen in October and November, with an unusually early development of the North Monsoon Current (e.g., Beal et al. 2013) associated with westward anomalies of  $\sim 30 \text{ cm s}^{-1}$  at  $3^{\circ}\text{S}$ – $2^{\circ}\text{N}$ ,  $60^{\circ}$ – $80^{\circ}\text{E}$  during these months (Fig. 3.20d). Large-scale current anomalies returned to near-climatological December values by the end of 2015.

The Agulhas Current transport is a key indicator of Indian–Atlantic Ocean interbasin water exchanges. The annual mean transport of the Agulhas Current has been decreasing from a high set in 2013, with values of 56 Sv in 2013 ( $1 \text{ Sv} \equiv 10^6 \text{ m}^3 \text{ s}^{-1}$ ), 53 Sv in 2014, and 50 Sv in 2015. The 2015 transport of 50 Sv is equal to the Agulhas’ long-term (1993–2015) mean.

Annual mean anomalies in the Atlantic Ocean (Fig. 3.19a) indicate a  $5$ – $7 \text{ cm s}^{-1}$  strengthening of the eastward NECC at  $4.5^{\circ}$ – $6.5^{\circ}\text{N}$ ,  $30^{\circ}$ – $50^{\circ}\text{W}$ , and conditions close to climatology along the equator. However, the annual average hides a pattern of reversing equatorial anomalies between boreal winter and spring (Fig. 3.20). The year began with eastward anomalies of  $20 \text{ cm s}^{-1}$  from  $3^{\circ}\text{S}$  to  $2^{\circ}\text{N}$  across much of the basin, which weakened through February and were present only at  $25^{\circ}$ – $35^{\circ}\text{W}$  in March/April. In May, westward anomalies of  $10$ – $15 \text{ cm s}^{-1}$  developed across the basin from  $2^{\circ}\text{S}$  to  $2^{\circ}\text{N}$ . These anomalies weakened considerably through June and were no longer present in July. No significant basinwide equatorial anomalies were seen in the remainder of 2015.

The Gulf Stream in 2015 remained close to its climatological position with little change from 2014 (Fig. 3.19).

The North Brazil Current, which sheds rings that carry waters from the Southern Hemisphere into the North Atlantic and has important ecosystem impacts downstream (Kelly et al. 2000), exhibited an annual transport smaller than its long-term (1993–2015) value. As in 2014, it shed eight rings in 2015, a larger-than-average value. Sea level anomalies in the region, which have generally increased since 2001

(apart from lows in 2003 and 2008), remained higher than average in 2015.

In the southwest Atlantic Ocean, the Brazil Current carries waters from subtropical to subpolar regions, mainly in the form of large anticyclonic rings (Lentini et al. 2006). The separation of the Brazil Current front from the continental shelf break continued to exhibit a seasonal cycle, which is mainly driven by wind stress curl variations and the transport of this current. During 1993–98, the annual mean separation of the front shifted southward in response to a long-term warming in South Atlantic temperatures (cf. Lumpkin and Garzoli 2010; Goni et al. 2011). In 2015, the Brazil Current front and its separation from the continental shelf break persisted south of its mean position, unchanged from 2014.

#### *h. Meridional overturning circulation observations in the North Atlantic Ocean—M. O. Baringer, M. Lankhorst, D. Volkov, S. Garzoli, S. Dong, U. Send, and C. S. Meinen*

This section describes the Atlantic meridional overturning circulation (AMOC) and the Atlantic meridional heat transport (AMHT), determined by the large-scale ocean circulation wherein northward moving upper layer waters are transformed into deep waters that return southward, redistributing heat, freshwater, carbon, and nutrients. Previous *State of the Climate* reports (e.g., Baringer et al. 2013) and reviews (e.g., Srokosz and Bryden 2015; Perez et al. 2015; Carton et al. 2014; Srokosz et al. 2012) discuss the AMOC’s impact on climate variability and ecosystems. The AMOC is computed as the maximum of the